HHS Public Access

Author manuscript

Curr Biol. Author manuscript; available in PMC 2020 April 01.

Published in final edited form as:

Curr Biol. 2019 April 01; 29(7): 1100–1111.e4. doi:10.1016/j.cub.2019.02.020.

Dynamic theta networks in the human medial temporal lobe support episodic memory.

Ethan A. Solomon[*,1], **Joel M. Stein**[2], **Sandhitsu Das**[2], **Richard Gorniak**[3], **Michael R. Sperling**[4], **Gregory Worrell**[5], **Cory S. Inman**[6], **Ryan J. Tan**[7], **Barbara C. Jobst**[8], **Daniel S. Rizzuto**[9], and **Michael J. Kahana**[*,9]

[1]Department of Bioengineering, University of Pennsylvania, Philadelphia PA 19104, USA

[2]Department of Radiology, Hospital of the University of Pennsylvania, Philadelphia PA 19104, USA

[3]Department of Radiology, Thomas Jefferson University Hospital, Philadelphia PA 19107, USA

[4]Department of Neurology, Thomas Jefferson University Hospital, Philadelphia, PA, 19107, USA

[5]Department of Neurology, Department of Physiology and Bioengineering, Mayo Clinic, Rochester, MN, 55905, USA

[6]Department of Neurosurgery, Emory School of Medicine, Atlanta GA 30322, USA

[7]Department of Neurosurgery, University of Texas Southwestern, Dallas, TX, 75390, USA

[8]Department of Neurology, Dartmouth Medical Center, Lebanon, NH, 03756, USA

[9]Department of Psychology, University of Pennsylvania, Philadelphia, PA, 19104, USA

Summary

The medial temporal lobe (MTL) is a locus of episodic memory in the human brain. It is comprised of cytologically distinct subregions that, in concert, give rise to successful encoding and retrieval of context-dependent memories. However, the functional connections between these subregions are poorly understood. To determine functional connectivity among MTL subregions, we had 131 subjects fitted with indwelling electrodes perform a verbal memory task, and asked how encoding or retrieval correlated with interregional synchronization. Using phase-based

[*]Corresponding Authors: Ethan A. Solomon, 425 S. University Ave., Levin Building, Rm. 201, Philadelphia, PA 19104, 631-252-1806, esolo@pennmedicine.upenn.edu; Michael J. Kahana, 425 S. University Ave., Levin Building, Rm. 201, Philadelphia, PA 19104, 215-746-3500, kahana@psych.upenn.edu.

Author Contributions E.S., M.J.K., and D.S.R. designed the study; E.S. analyzed data, and E.S. wrote the paper. J.S., R. Gorniak, S. Das. performed anatomical localization of depth electrodes. M.S., G.W., R.T., C.I., B.J. recruited subjects, collected data, and performed clinical duties associated with data collection including neurosurgical procedures or patient monitoring.

Lead Contact: Michael J. Kahana, kahana@psych.upenn.edu

Declaration of Interests

The authors declare no competing interests.

Data and software availability

Raw electrophysiogical data used in this study is freely available at http://memory.psych.upenn.edu/Electrophysiological_Data

measures of connectivity, we found that synchronous theta (4-8 Hz) activity underlies successful episodic memory. During encoding, we observed a dynamic pattern of connections converging on the left entorhinal cortex, beginning with the perirhinal cortex and shifting through hippocampal subfields. Retrieval-associated networks demonstrated enhanced involvement of the subiculum and CA1, reflecting a substantial reorganization of the encoding network. We posit that coherent theta activity within the MTL marks periods of successful memory, but distinct patterns of connectivity dissociate key stages of memory processing.

eTOC Blurb

The medial temporal lobe (MTL) is key to episodic memory, but little is known about communication between its subparts. Solomon et al. analyze phase relations between MTL subregions in 131 humans with depth electrodes, identifying the entorhinal cortex as a hub of theta connectivity during encoding, and a reorganized network supporting retrieval.

Introduction

Storing episodic memories is an inherently integrative process, long conceptualized as a process that links information about new items to an observer's current thoughts, emotions, and environment [1]. Decades of behavioral observations, clinical case studies, and neural recordings in humans have shed light on the key principles and diverse set of brain structures underlying this integration, including frontal, lateral temporal, and medial temporal cortex (MTL) [2]. Recent hypotheses invoke the idea that communication among these regions supports memory formation, spurred by a growing number of functional imaging and intracranial electroencephalography (iEEG) experiments that show synchronized activity among the MTL and cortical structures during memory tasks [3–6].

However, the MTL has a unique role in supporting episodic memory. Damage to the MTL results in profound deficits of memory [7], and it has been shown to exhibit enhanced neural activity during memory processing in a range of tasks and experimental models [8,9], identifying this area as a key anatomic hub of episodic encoding and retrieval. The MTL is structurally complex; it is subdivided into hippocampus, rhinal cortex, and parahippocampal cortex. The cornu ammonis (CA), dentate gyrus, and subiculum comprise the hippocampus, while the entrorhinal and perirhinal cortices form the rhinal cortex. Microscale recordings in animals have revealed that these substructures exhibit distinct patterns of activity during memory and navigation tasks, including the generation of oscillations, inter-regional synchronization, and neuronal selectivity for time and space [10–16]. Computational models of MTL function have assigned unique roles to MTL substructures, pertaining to episodic encoding, retrieval, or recognition [10,17–20] – typically, these models suggest extrahippocampal regions are responsible for placing sensory inputs in a useful representational space, while the hippocampus itself forms associative links between these representations and their prevailing context.

Virtually all of the aforementioned animal and modeling literature suggests that MTL substructures communicate with one another as they engage in memory processing. However, the volume of aforementioned work on intra-MTL connectivity has not been

matched by validation studies in humans. Though a handful of investigations have begun to address this question in neurosurgical patients [21–23], limited electrode coverage and coarse localizations have made it difficult to study the complete extent of neural synchronization within the MTL, including the role of functionally distinct subregions. But doing so is necessary to validate models of MTL function that suggest communication among specific regions – such as between subdivisions of rhinal cortex and hippocampus – supports computations necessary for associative memory formation and retrieval.

The use of intracranial depth electrodes to study neural activity in the MTL also allows neural activity to be studied at different timescales. Slow theta (4-8 Hz) oscillations in the hippocampus have been observed during memory processing in humans [24–26], as have fluctuations at higher frequencies, including the gamma (30-60 Hz) band [27,28]. These oscillations have been theorized to support synchronization between neural assemblies in the MTL [15,17,29–31], but MTL connectivity has not been fully mapped across frequency bands. The extent to which different frequencies underlie neural synchronization in memory therefore remains an open question, though converging lines of evidence strongly suggest the most prominent connectivity effects occur at low frequencies [32–36].

In this study, we aimed to define the patterns of functional connectivity that emerge in the human MTL and to specifically characterize how MTL-subregional connectivity differs when memories are being stored versus when they are being subsequently retrieved. We leveraged a large dataset of 131 subjects with depth electrodes placed in the MTL, localized with hippocampal subfield resolution, and focused on two key contrasts: (1) the encoding subsequent memory effect (SME), differentiating remembered from forgotten items, and (2) successful retrieval versus periods of unsuccessful memory search. We found that successful encoding was characterized by dynamic cascade of low-frequency connections to the left entorhinal cortex, while retrieval was associated with enhanced theta connectivity involving subiculum and CA1. However, these differing connectivity patterns were not correlated with markedly different patterns of local spectral power between encoding and retrieval, suggesting functional connections are a key mechanism by which the MTL may switch between distinct memory operations. Taken together, our findings show that low-frequency functional coupling in the MTL supports the formation of new memories, with the specific pattern of connections acting as the key determinant of successful encoding and retrieval, respectively.

Results

Our general approach to characterizing intra-MTL connectivity was to (1) examine the structure of functional connectivity networks using graph-theoretic analysis, (2) examine the timecourse of connectivity in key connections, and (3) relate changes in connectivity to changes in local activity, as reflected by spectral power. To do this, we correlated intra-MTL synchronization with memory state using two contrasts in a verbal free-recall paradigm. First, we examined the subsequent memory effect (SME), which has been widely employed to characterize whole-brain modulations of spectral power (e.g. [28,37]) that correlate with successful memory encoding. Second, we examined a memory retrieval contrast, wherein epochs of time leading up to verbalization of a recalled item are compared to matched

epochs of time, from other word lists, where no recall occurs (e.g. 29, 40, 41; see Methods for details). We refer to these matched periods as “deliberation” intervals.

For each contrast, we constructed intra-MTL functional connectivity maps at each frequency band using the phase-locking value (PLV). The PLV [40] is used to assess whether, across trials, there is a consistent phase difference between two electrodes. We had 131 subjects perform a verbal free-recall task during which iEEG was collected from depth electrodes placed in the MTL. Electrodes were localized to hippocampal subfields determined by the Automatic Segmentation of Hippocampal Subfields (ASHS) algorithm [60], by co-registering postoperative CT scans to pre-operative T2 MRI. Subjects were serially presented with 12-item word lists and asked to recall as many words as possible after a brief distractor task (Figure 1A-C; see Methods for details). For each electrode pair, phase differences were computed for each trial, i.e. an encoding or retrieval event. Trials were sorted by whether a word was later recalled or forgotten (or, in the retrieval contrast, a successful retrieval event or matched deliberation; Figure 1D). PLV was computed for successful/unsuccessful groups separately, and tested for significant differences via a nonparametric permutation procedure (see Methods for details). Effects were averaged across electrode pairs, subjects, and time, yielding a z-score that indicates the relative synchronization in successful vs. unsuccessful memory encoding/retrieval for each pair of MTL regions (see Figure 2A for an example pair; see Figure S1 for subject/electrode count per region-pair). We used the common average reference (restricted to MTL electrodes), as large inter-electrode spacing makes the bipolar reference a poor choice for studies of intra-MTL synchronization (see Methods for further discussion).

Theta networks of memory encoding and retrieval.

Given strong evidence in the literature for synchronous memory effects in the theta band [32–36], we first sought to characterize the detailed structure of theta (4-8 Hz) networks in the MTL. First, we constructed the adjacency matrix representation of intra-MTL functional connectivity for each contrast, reflecting memory-related theta synchrony between any possible pair of subregions as a z-score (Figure 2A-B). Next, we asked whether any regions acted as “hubs” of the MTL by computing the node strength for each region, using theta PLV connection weights. Node strength reflects the overall connectivity to a given node of the network by summing all of its connection weights. In the SME contrast, left entorhinal cortex emerged as a significant hub (corrected permuted $P < 0.05$; Figure 2D). In the retrieval contrast, left CA1 was numerically greatest and significant if not corrected for multiple comparisons (permuted $P = 0.013$; Figure 2F). The single strongest connection for the encoding/retrieval contrasts were EC-PRC ($Z = 2.65$) and CA1-Sub ($Z = 2.00$), respectively (see Figure 1 legend for region abbreviations). For each contrast, the strongest synchronous connections are depicted schematically in Figures 2C and 2E. In both retrieval and encoding, entorhinal cortex exhibits enhanced connectivity to CA1 and subiculum, with additional perirhinal-hippocampal connections present exclusively in encoding. Additionally, in both contrasts, connections within the left MTL are significantly greater than zero (encoding, permuted $P = 0.005$; retrieval, $P = 0.04$), and stronger than connections within the right MTL, though not significantly so for encoding (encoding, permuted $P = 0.15$; retrieval, $P = 0.03$).

These findings align with known anatomical connections and functional roles of MTL subregions. The entorhinal cortex acts as a key input structure to the hippocampus and represents the convergence of information from the perirhinal and parahippocampal cortices [41,42] – it is fitting that this structure exhibits enhanced theta connectivity to other MTL structures during with successful memory encoding. Furthermore, a reorganization of theta networks featuring enhanced connectivity between the subiculum and CA1 comports with anatomical connectivity and notion of subiculum's role as a major output structure of the hippocampus [43,44]. However, this initial network-based analysis averages synchrony effects over the entire word presentation or retrieval intervals, obscuring potentially significant time-varying dynamics.

Temporal dynamics of memory-related theta connectivity.

Having shown that encoding- and retrieval-associated theta networks differ in their structure but align with known anatomical connectivity of the MTL, we next asked whether our previously-identified synchronous connections exhibited time-varying dynamics. To do this, we assessed inter-regional theta in the left MTL – noted earlier to have stronger ipsilateral coupling than the right MTL – during three epochs of the encoding period (400 ms bins from 0-1200 ms after word onset) and two epochs of the retrieval period (500 ms bins). This analysis revealed divergent patterns of connectivity between temporal epochs. During successful relative to unsuccessful encoding, we found an early (400-800 ms) synchronization between left EC and left PRC (Z = 2.79), followed by EC-CA1 synchronization ($Z = 3.21$), and ending with a late-stage synchronization between subiculum and EC ($Z = 2.13$; Figure 3A). Successful retrieval was characterized by an early left DG-subiculum and CA-PHC coupling (permuted $P < 0.05$), followed by left CA1 connectivity to both subiculum and EC immediately prior to retrieval onset ($P < 0.05$; Figure 3B).

These findings underscore why we identified the left EC as a hub of theta connectivity during successful memory encoding – a cascade of theta coupling to the left EC plays out over the course of the encoding interval. It begins with synchronization between PRC and EC in the −100-300 ms interval (permuted $P < 0.05$), shifts to CA1 and DG (400 ms to 900 ms across both), and ends with subiculum (900 to 1200 ms). The timecourses for each of these key connections are depicted in Figure 4, along with their corresponding time-frequency spectrogram contrasts. Though the PLV is a non-directional measure, the timing of these connections suggest a flow of activity through the MTL; initially, cortical inputs arrive to the EC via the PRC, which subsequently synchronizes with the DG and CA1 via the perforant pathway. The final EC-Sub synchronization could reflect inputs from EC or hippocampal outputs (i.e. a retrieval process overlapping the encoding interval).

The PLV captures consistent phase differences between electrodes across trials, but it provides no direct quantification of the magnitude of phase lags themselves. However, the phase lag is pertinent to the meaning of inter-regional synchronization, particularly if the lags are at or near zero, which may indicate volume conduction [45,46] or true physiologic coupling [6]. In light of this, we assessed the magnitude of phase differences associated with increased connectivity for the key connections between left EC and other MTL subregions. Small mean phase lags (< 5 degrees) were noted in a subset of electrode pairs (i.e. 24% of

pairs between EC-CA1 and 25% of pairs between EC-PRC), but memory-related synchronization was not significantly higher for such pairs (2-sample t-test; $P > 0.05$; Figure S2 and Figure S3). We further noted a general decrease in the magnitude of phase lags in successful encoding trials relative to unsuccessful encoding, though the effect was more pronounced for lags with a high magnitude at baseline (Figure S2-A). Taken together, the magnitude of phase lags underlying successful encoding span a wide range, but there is no evidence to suggest near-zero lags primarily drive an increase in observed connectivity.

We also observed changes in theta connectivity over the course of the pre-retrieval period (Figure 5). Most prominently, we observed a significant increase coupling in the several hundred milliseconds immediately preceding retrieval onset; left CA1 and subiculum (−200 to 0 ms) and CA1-EC (−300 to −100 ms). In these connections, we again noted a relative decrease in the magnitude of phase lags in successful retrieval versus deliberation intervals (Figure S2-C), but found no evidence that zero-lag differences were driving measures of enhanced connectivity (Figure S2-D). In a separate analysis, we used the weighted phase-lag index (wPLI) to assess intra-MTL synchronization while downweighting lags close to zero (Figure S4) [45]. We failed to find network-wide theta synchronization using this conservative metric (e.g. Figure S4-H), likely reflecting the relative shift in phase lags between successful and unsuccessful memory (see Discussion).

Taken together, theta networks within the left MTL exhibit time-varying structure, including a cascade of functional connectivity to the left EC which suggests a neocortical-EC-hippocampal flow of activity. This is in accordance with prior work across several modalities [19,29,47], though we have demonstrated here that this circuit is observable via changes in theta connectivity. Connectivity, however, is only half the story – are changes in intra-MTL connectivity associated with modulations of local activity in these same regions?

Relationship between connectivity and spectral power.

Our primary focus was to characterize patterns of intra-MTL connectivity, but it is known that MTL subregions exhibit distinct patterns of local activation associated with episodic memory [48,49]. We therefore asked whether changes in local spectral activity within the MTL correlate with encoding and retrieval states, and whether such changes relate to inter-regional theta connectivity. To do this, we analyzed the relative spectral power between successful and unsuccessful encoding/retrieval trials, in the theta band (4-8 Hz) and frequencies that correspond to high-frequency activity (HFA, 30-90 Hz). HFA is established as a general marker of neural activation that likely includes gamma oscillatory components and spectral leakage from aggregate unit spiking activity [50]. For each MTL subregion, we computed the power SME and retrieval contrast for each electrode at each frequency, and averaged these effects across electrodes and subjects (see Methods for details). This procedure results in a *t*-statistic that reflects the relative power in a given region between successful and unsuccessful encoding/retrieval events.

Though we broadly observed positive theta connectivity associated with successful episodic memory, spectral power contrasts at the same frequencies went in the opposite direction. Bilateral CA1 and PRC exhibited significant decreases in theta power associated with successful encoding, as did left DG, left PHC, and right subiculum (1-sample *t*-test; FDR-

corrected $P < 0.05$; Figure 6A). Bilateral CA1 also exhibited significantly enhanced HFA, and HFA was otherwise nonsignificantly increased in all MTL regions. Power dynamics associated with successful retrieval were similar to those observed in the encoding contrast. Theta was generally decreased in the left MTL, significantly so in left PRC and CA1 (FDR-corrected $P < 0.05$). Furthermore, HFA was elevated in bilateral CA1 and DG. The general trend of decreased theta power and increased HFA aligns with a robust literature demonstrating this same effect across a diverse array of cortical regions and the MTL [3,27,28,51].

Between left EC and CA1, which exhibited strong memory-related increases in theta connectivity, we asked whether there was a relationship between modulations of spectral power and connectivity. During successful encoding, left CA1 showed a significant (1-sample t-test; $P < 0.05$) increase in HFA from 700-900 ms after word onset, coincident with the 500-800 ms theta connectivity to EC shown in Figure 5B (Figure 6B, top row). Additionally, CA1 exhibited a sustained and significant decrease in theta power beginning at 500 ms, while EC showed a transient decrease from 200 to 600 ms (no significantly increased HFA was observed in EC). In the retrieval contrast, HFA increased and theta power decreased in CA1 prior to onset of a successfully retrieved word (HFA, −600-0 ms prior to onset; theta, −300-0 ms). Both of these intervals overlapped with the period of enhanced CA1-EC theta synchrony from −300 to −100 ms (Figure 6C). We did not find significant modulations of power in either band in EC during retrieval, but noted subthreshold increases in HFA and decreases in theta power in the preretrieval interval (Figure 6C, right panel). Time-frequency analyses for all MTL regions are reported in Figures S5. Collectively, these results recapitulate a theme noted in an earlier study of whole-brain connectivity [3]: Increases in low-frequency connectivity are often associated with increases in high-frequency power and decreases in low-frequency power.

In other cases, there is little evidence for a strict power-synchrony relationship. Unlike the patterns of theta connectivity described earlier (Figures 3–5), we did not observe a cascade of activity through the MTL when examining spectral power alone. For example, though we previously noted early EC-PRC and late EC-Sub synchronization during encoding, no significant fluctuations in spectral power occur in these regions during those times (Figure S5). Instead, almost every MTL subregion is characterized by a general spectral tilt of decreased low-frequency power and increased high-frequency power that begins between 300 ms and 500 ms after word onset, or about 500 ms prior to retrieval onset. These findings suggest that, in the average, theta connectivity reveals patterns of memory-related activation in the MTL which are not also observable through traditional power analyses.

Memory effects by frequency band.

As several frequency bands have been implicated in intra-MTL synchronization [10,23,33,52,53] – notably theta (4-8 Hz) and low gamma (30-60 Hz) – we finally asked whether memory-related connectivity in the MTL was also present at higher frequency bands. For the theta, alpha (9-13 Hz), beta (16-28 Hz), and low gamma bands, we only observed significant network-wide increases in connectivity in the left MTL during encoding (FDR-corrected permuted $P < 0.05$; Figure 7A; see Methods for details). An increase in

theta connectivity was also observed in the left MTL during retrieval, as noted earlier (Figure 2), but did not reach significance when corrected for multiple comparisons. Specific connection weights for each contrast are depicted in Figure 7B. In general, synchronization tended to decrease with increasing frequency – networks computed at beta and gamma frequencies were net negative in both hemispheres and task contrasts, except for the right MTL during encoding.

To address recent work that has examined especially low and high frequencies in the MTL [54–56], we expanded our original analysis to ask about network-wide synchronization in the low theta (1-3 Hz) and high gamma (70-90 Hz) bands. FDR-corrected for multiple comparisons, we found significant (permuted $P < 0.05$) low-theta connectivity within the left MTL for the encoding SME and retrieval contrasts (Figure S6-A). These findings were generally driven by increases in rhinal-hippocampal coupling for both contrasts (Figure S6-B). Networks constructed from high gamma activity were not significantly elevated for either hemisphere or task contrast.

Taken together, we only observed network-wide increases in MTL connectivity in the theta and low-theta bands, particularly in the left hemisphere. It is possible that specific connections are individually significant at higher frequencies, but the underlying mix of synchronous and asynchronous connectivity yields a nonsignificant network-wide measure. We avoided further tests to not risk inflating our Type I error rate in this exploratory study, though future studies may consider hypothesis driven tests of specific connections.

Discussion

We set out to understand neural interactions between substructures of the MTL during episodic encoding and retrieval. As 131 subjects performed a verbal free-recall task, we recorded intracranial EEG from the MTL and compared inter-regional connectivity between periods of successful and unsuccessful memory operations. Using these methods, we discovered that theta phase locking marks periods of successful memory encoding and retrieval, with left entorhinal cortex acting as a key hub for theta connectivity during encoding, and a reorganized left-MTL network supporting retrieval. Furthermore, connections to the left EC were dynamic, migrating from an initial EC-PRC coupling, followed by EC-CA1/DG, and ending with EC-subiculum. Concurrent with these findings was a general decrease in theta power and increase in high-frequency activity in both retrieval and encoding, though the degree of power modulation was not strictly correlated with patterns of theta connectivity.

Our identification of encoding and retrieval-associated networks enriches computational models of memory in the MTL. An influential theory of MTL function postulates that theta oscillations within the hippocampal-entorhinal system constitute a common substrate of navigation and episodic memory, by facilitating synaptic plasticity, coordinating neural ensembles, and synchronizing EC representations of physical or mental space with hippocampal mechanisms that serve to neurally associate these representations with context [18,19,29,31,33,57]. In support of this theory, we found that theta connectivity between the EC and CA1/DG was predictive of successful episodic encoding, and theta coupling

between the EC and hippocampus occurred alongside increased high-frequency hippocampal power. The early period of enhanced theta connectivity between EC and PRC has not been reported before in humans but supports the notion that EC's representations are built on sensory input from the neocortex, routed through extrahippocampal MTL regions.

Our findings also indicate a role for theta synchronization during memory retrieval. Indeed, as suggested by anatomical evidence [43] and models of hippocampal function [58], successful retrieval was associated with enhanced connectivity between CA1-EC and CA1-subiculum. Both of these functional connections may support the reinstatement of neocortical activity associated with contextually-retrieved information, driven by pattern completion in CA3. The identification of late-stage subiculum-EC coupling in the encoding contrast might suggest an overlapping retrieval processes that occurs after initial learning, so as to link the current item with previously-experienced ones.

However, the relationship between inter-regional theta synchronization and local activity is not straightforward. Though the prominent EC-CA1 connection is temporally associated with increased HFA and decreased theta power (in encoding and retrieval), the early EC-PRC connectivity and late EC-subiculum connection do not coincide with notable alterations of spectral power. Moreover, why is theta power generally decreased while theta connectivity is generally increased? Two possibilities deserve future consideration: (1) many electrodes exhibit task-related decreases in theta power and no change in inter-regional connectivity, but a subset exhibit strong theta coupling and increases in theta power. The resulting picture, on average, is enhanced connectivity and weakened/unaltered power. (2) Any electrode with enhanced connectivity also exhibits decreased power, because slight drawdowns in power are necessary to accomplish inter-regional phase locking. The memory contrasts (e.g. SME) reflect decreases in theta power, even though baseline levels of theta power remain high.

In this study, we addressed the potential confound of volume conduction by assessing the magnitude of phase lags between pairs of electrodes. Though near-zero lags were present in the data, they were not associated with a relative increase in phase synchronization, which would be expected if volume conduction were driving spurious increases in connectivity. Indeed, zero-lag differences at low frequencies may play an important mechanistic role [6], though we do note that zero-lag differences at higher frequencies (60+ Hz) are less biophysically plausible [30]. We further considered use of the wPLI, which corrects for potential volume conduction by discounting small phase lags [45]. However, use of this statistic raises interpretive difficulties, as it reduces the ability to detect true coupling with small phase lags. Also, the wPLI indicates relative decreases in synchronization between task conditions if (1) phase lag distributions becomes more dispersed or (2) phase lags rotate towards zero, while maintaining constant concentration (Cohen, 2015; see Figure S4). Finally, it is not clear that volume-conducted field potentials should even be "corrected" for – fields detectable by an electrode are detectable by neurons, and they may yet be shown to serve an important role in inter-regional communication.

Our use of a verbal free-recall task – though a powerful paradigm for studying episodic memory – necessitated the construction of a retrieval contrast that merits further discussion.

In this manuscript, we compared neural activity in 1-second intervals leading up to vocalization of a word against 1-second intervals at matched periods of time with no recalls, in free-recall periods from other lists. In this way, we aimed to contrast activity related to successful retrieval against activity during which subjects were liable to try, but fail, to recall a word. This paradigm has been employed in several prior studies examining the neural correlates of free recall [3,28,38,39]. However, free-recall tasks inherently confound neural process responsible for episodic retrieval with processes responsible for vocalization and motor preparatory behavior. To account for this, our analyses exclusively consider the MTL – not canonically associated with speech preparation – and only examine activity in the time period preceding onset of vocalization. It is still possible that speech-related activity contaminates the retrieval contrast reported here – other possible contrasts could leverage nonword vocalizations or intrusion events, though these are typically too rare to serve as a statistically valid basis for connectivity computations. Replicating the finding of recalled-associated theta synchrony in a cued-recall paradigm would therefore be a valuable complement to this work.

In this study, we did not find strong evidence for memory-related gamma synchronization within the MTL. However, earlier reports of hippocampal-rhinal connectivity in humans have reported effects in the gamma band [21,23], and animal work also suggests inter-regional gamma coherence is present in the MTL [30,54,55]. To constrain our hypothesis space, we did not statistically assess any possible gamma-band synchronization in detail, though our time-frequency analyses of key hippocampal-rhinal connections such as EC-CA1 and EC-DG do not qualitatively indicate robust increases in gamma synchronization associated with successful encoding (see Figure 4B). Future studies should ask whether specific predictions of intra-MTL gamma coherence hold true during episodic memory processing in humans.

In summary, we found that theta band connectivity characterizes intra-MTL interactions that are related to memory encoding and retrieval processes, but distinct networks correlate with successful encoding and retrieval. During encoding, we found EC to be a hub of theta connectivity, driven by an evolving cascade of connections to almost every other part of the MTL. During retrieval, we observed a reorganized theta network, with no clear hubs but enhanced connectivity between EC-CA1 and CA1-subiculum. Connectivity patterns revealed subregional involvement in memory processing that were not observable by an analysis of spectral power alone. These findings point to theta interactions as the key to unlocking the way in which medial temporal structures give rise to episodic memories.

STAR Methods

Contact for reagent and resource sharing

Further information and requests for resources and reagents should be directed to and will be fulfilled by the Lead Contact, Michael J. Kahana (kahana@psych.upenn.edu).

Experimental model and subject details

Human subjects—For connectivity analyses, 131 adult (mean age 38.8 yrs, standard deviation 11.7 yrs; 68 female) patients with medication-resistant epilepsy underwent a surgical procedure to implant subdural platinum recording contacts on the cortical surface and within brain parenchyma. Gender differences were not assessed in this study. Statistical comparisons between memory conditions were done within-subject for this study, necessitating no separation into multiple experimental groups. *Sample size estimation:* Any subject at participating clinical sites was included in this study if they had depth electrodes placed in one or more MTL subregion and were willing to complete at least one experimental session.

Contacts were placed so as to best localize epileptic regions. Data reported were collected at 8 hospitals over 3 years (2015-2017): Thomas Jefferson University Hospital (Philadelphia, PA), University of Texas Southwestern Medical Center (Dallas, TX), Emory University Hospital (Atlanta, GA), Dartmouth-Hitchcock Medical Center (Lebanon, NH), Hospital of the University of Pennsylvania (Philadelphia, PA), Mayo Clinic (Rochester, MN), National Institutes of Health (Bethesda, MD), and Columbia University Hospital (New York, NY). Prior to data collection, our research protocol was approved by the Institutional Review Board at participating hospitals, and informed consent was obtained from each participant.

Method details

Free-recall task—Each subject participated in a delayed free-recall task in which they studied a list of words with the intention to commit the items to memory. The task was performed at bedside on a laptop. Analog pulses were sent to available recording channels to enable alignment of experimental events with the recorded iEEG signal.

The recall task consisted of three distinct phases: encoding, delay, and retrieval. During encoding, lists of 12 words were visually presented. Words were selected at random, without replacement, from a pool of high frequency English nouns (http://memory.psvch.upenn.edu/WordPools). Word presentation lasted for a duration of 1600 ms, followed by a blank inter-sitmulus interval of 800 to 1200 ms. Before each list, subjects were given a 10-second countdown period during which they passively watch the screen as centrally-placed numbers count down from 10. Presentation of word lists was followed by a 20 second post-encoding delay, during which time subjects performed an arithmetic task during the delay in order to disrupt memory for end-of-list items. Math problems of the form A+B+C=?? were presented to the participant, with values of A, B, and C set to random single digit integers. After the delay, a row of asterisks, accompanied by a 60 Hz auditory tone, was presented for a duration of 300 ms to signal the start of the recall period. Subjects were instructed to recall as many words as possible from the most recent list, in any order, during the 30 second recall period. Vocal responses were digitally recorded and parsed offline using Penn TotalRecall (http://memory.psych.upenn.edu/TotalRecall). Subjects performed up to 25 recall lists in a single session (300 individual words).

Electrocorticographic recordings—iEEG signal was recorded using depth electrodes (contacts spaced 2.2-10 mm apart) using recording systems at each clinical site (see Table

S1 for recording contact sizes). iEEG systems included DeltaMed XlTek (Natus), Grass Telefactor, and Nihon-Kohden EEG systems. Signals were sampled at 500, 1000, or 1600 Hz, depending on hardware restrictions and considerations of clinical application. Signals recorded at individual electrodes were first referenced to a common contact placed intracranially, on the scalp, or mastoid process. To eliminate potentially confounding large-scale artifacts and noise on the reference channel, we next re-referenced the data using the common average of all depth electrodes in the MTL that were used for later analysis. Signals were notch filtered at 60 Hz with a fourth-order 2 Hz stop-band butterworth notch filter in order to remove the effects of line noise on the iEEG signal, and downsampled to 256 Hz. Event-related potentials (ERPs) were not subtracted.

As determined by a clinician, any contacts placed in epileptogenic tissue or exhibiting frequent inter-ictal spiking were excluded from all subsequent analyses. Any subject with fewer than 3 remaining recording contacts in the MTL were not included in the analysis. Any subject with fewer than 15 trials of successful encoding or successful retrieval (see "Retrieval analyses") were excluded from analysis (encoding, 3 subjects excluded; retrieval, 21 subjects excluded).

Limitations of the bipolar reference: In this manuscript, we only used the common average reference (restricted to electrodes in the MTL). While it would also be possible to use the bipolar reference, its use in studies of intra-MTL connectivity is limited by the geometry of linear depth electrodes relative to MTL structures; it is often the case that a bipolar midpoint "virtual" electrode will fall in a subregion/subfield where neither physical contact was placed, raising interpretive difficulties. Additionally, connectivities between bipolar electrodes that share a common monopolar contact are contaminated by shared signal between the two – ideally, such pairs should be excluded from analysis. However, doing so drastically reduces the number of possible region-to-region pairs within the MTL.

Anatomical localization—To precisely localize MTL depth electrodes, hippocampal subfields and MTL cortices were automatically labeled in a pre-implant, T2-weighted MRI using the automatic segmentation of hippocampal subfields (ASHS) multi-atlas segmentation method [60]. Post-implant CT images were coregistered with presurgical T1 and T2 weighted structural scans with Advanced Normalization Tools [61]. MTL depth electrodes that were visible on CT scans were then localized within MTL subregions by neuroradiologists with expertise in MTL anatomy. Exposed recording contacts were approximately 1-2mm in diameter and 1-2.5mm in length; the smallest recording contacts used were 0.8mm in diameter and 1.4 mm in length (see Table S1 for all electrode dimensions). MTL diagrams were adapted with permission from Moore, et al. [62]. See Figure S1 for examples of coregistered CT/T2-MRI which depict depth electrodes and overlaid segmentations derived from ASHS.

Quantification and statistical analysis

Data analyses and spectral methods—Of the 131 subjects in this study, 120 had electrodes placed in more than one MTL subregion and were included connectivity analyses. To obtain phase-locking values (PLV) and weighted phase lag index (wPLI; see Figure S4)

between electrode pairs, we used the MNE Python software package [63], a collection of tools and processing pipelines for analyzing EEG data. PLV reflects the consistency of phase differences between two electrodes across trials [40]. wPLI operates similarly to PLV, but weights phase differences according to their rotation away from the zero axis, to account for volume conduction [45]. Stated differently, the wPLI weights cross-spectra by the magnitude of the imaginary component of the cross spectrum. Therefore, maximum wPLI is achieved if phase differences are tightly clustered around 90 (or 270) degrees. Both metrics range from 0 (no synchronization) to 1 (maximal synchronization).

To obtain phase information, we convolved signals from each MTL recording contact with compelx-valued Morlet wavelets (6 cycles). We used 24 wavelets from 3-60 Hz as follows: theta (4-8 Hz, spaced 1 Hz), alpha (9-13 Hz, spaced 1 Hz), beta (16-28 Hz, spaced 2 Hz), low gamma (30-60 Hz, spaced 5 Hz). Extended frequency bands (Figure S6) included low theta (1-3 Hz) and high gamma (70-90 Hz). For encoding analyses, each wavelet was convolved with 4000 ms of data surrounding each word presentation (referred to as a "trial"), from 200 ms prior to word onset to 1800 ms afterwards, buffered with 1000 ms on either end (clipped after convolution). Retrieval analyses considered 1000 ms of data prior to each retrieval event, also buffered with 1000 ms on either end. (Low-theta supplemental analyses used 2000 ms buffers and 3 cycle wavelets.)

For each subject, for all possible pairwise combinations of MTL electrodes, we compared the distributions of phase differences in all remembered trials against all not-remembered trials, asking whether there is a significantly higher PLV/wPLI in one or the other. In the encoding contrast, values were compared between all epochs where words were later remembered versus forgotten. In the retrieval contrast, values were compared between epochs leading up to onset of a verbal recall versus matched periods of time when no recall occurred ("deliberation" events, see "Retrieval analysis"). To do this, we found the difference of PLV/wPLI across conditions, e.g.:

$$D_{pq}(f,t) = PLV_{rem} - PLV_{nrem} \quad (1)$$

Where pq is an electrode pair, f is a frequency of interest, and t is a window in time. Higher positive differences (D) indicate greater connectivity for remembered trials, whereas lower negative differences reflect greater connectivity for not-remembered trials. D was computed for each frequency spanning a range from 3 to 60 Hz, averaged into 100 ms non-overlapping windows spanning each trial (i.e. word encoding or pre-retrieval event). 20 windows covered encoding events, from 200 ms prior to word onset to 200 ms after offset. 10 windows covered retrieval/deliberation events, starting 1 second prior to word onset (or 1-second of time during matched deliberation period).

PLV and wPLI values are biased by the number of vectors in a sample. Since our subjects generally forget more words than they remember, we adopt a nonparametric permutation test of significance. For each subject, and each electrode pair, the synchrony computation described above was repeated 250 times with the trial labels shuffled, generating a distribution of D statistics that could be expected by chance for every electrode pair, at each

frequency and time window. Since only the trial labels are shuffled, the relative size of the surrogate remembered and not-remembered samples also reflect the same sample size bias. Consequently, the true D (D_{true}) can be compared to the distribution of null Ds to derive a z-score or p-value. Higher z-scores indicate greater synchronization between a pair of electrodes for items that are successfully recalled.

To construct a network of synchrony effects between all MTL subregions, we pooled synchrony effects across electrode pairs that span a pair of subregions, and then pooled these subregion-level synchronizations across subjects with that pair of subregions sampled. To do this, we first averaged the D_{true} values across all electrode pairs that spanned a given pair of subregions within a subject. Next, we averaged the corresponding null distributions of these electrode pairs, resulting in a single D_{true} and a single null distribution for each subregion-pair in a subject. We then averaged the Dtrue values and null distributions across all subjects with electrodes in a given ROI pair. By comparing the averaged D_{true} to the averaged null distribution, we computed a z-score (and corresponding p-value) at each frequency and temporal epoch that indicates significant synchrony or asynchrony, depending on which tail of the null distribution the true statistic falls.

Statistical considerations: Our procedure for averaging the true and null statistics across subjects enables us to construct whole-MTL networks across datasets in which no single subject has electrodes in every region of interest. We compute statistics on these networks that leverage their completeness, including overall connection strength and node strengths (Figure 2, Figure 7). Such statistics cannot be assessed at the level of individual subjects who may only have electrode pairs that span a small subset of MTL regions. However, the connection strengths for individual region-pairs can be statistically evaluated across subjects using a 1-sample T-test, so long as a sufficient number of subjects have been sampled for that pair. To demonstrate the correspondence between these two approaches, we correlated the connection weight of population-level z-scores (derived from the permutation procedure above) to t-statistics computed derived from a 1-sample T-test on z-scores from individual subjects. Across all possible region-pairs, connection weights are highly correlated between the two methods (Pearson'r $r = 0.88$).

Network analyses—Using the population-level statistics described above, a 12-by-12 adjacency matrix was constructed for each of the temporal epochs in encoding/retrieval conditions, for each frequency. This matrix represented every possible interaction between all MTL subregions. The z-score of the true D relative to the null distribution was used as the connection weight of each edge in the adjacency matrix. Negative weights indicate ROI pairs that, on average, desynchronized when a word was recalled successfully, and positive weights indicate ROI pairs that synchronized when a word was recalled successfully. We zeroed-out any ROI pairs in the matrix represented by less than 5 subjects' worth of data, to limit the likelihood that our population-level matrix is driven by strong effects in a single or very small number of individuals (see Figure S1 for subject and electrode counts at each pair).

Since it is possible that collections of weaker connection weights may still account for significant structure in our network, we did not apply a z-score threshold before further

analyses. To assess for the significance of phenomena at the network level, we instead used 250 null networks that can be constructed on the basis of *D*s derived from the shuffled trial labels to generate a distribution of chance network-level statistics. True statistics were compared to these null distributions to obtain a P-value or z-score (e.g. network-wide summed connections weights were computed for true and null networks and reported in Fig. 2A-B).

Adjacency matrices reflect the average connectivity strength during the item presentation interval (0-1600 ms) or retrieval period (−1000-0 ms) for each frequency band. To create them, we averaged true connection strengths within frequency bands, then averaged across all the 100 ms time windows in the encoding/retrieval intervals, and compared the result to the time/frequency average from each of the 250 null networks, resulting in a new Z-score for the time/frequency-averaged network (e.g. Figure 2A).

In analyses of connectivity timecourses (Figures 3–5), intervals are marked as significant so long as the p-value of PLV/wPLI connectivity exceeds a threshold of $P < 0.05$ (relative to the null distribution for that epoch) for at least 2 consecutive 100 ms epochs.

Hub analysis—To determine which MTL regions act as significant “hubs,” or regions that have enhanced connectivity to many other nodes in the network, we use the node strength statistic from graph theory (Equation 2) [64]:

$$k_i^w = \Sigma_{j \in N} w_{ij} \quad (2)$$

Where k is the node strength of node i, and w_{ij} refers to the edge weight between nodes i and j. N is the set of all nodes in the network. In this paper, we only use ipsilateral MTL regions to compute the node strength of each region, so as to (1) better reflect the engagement of a region with its immediate neighbors and (2) acknowledge the sparser sampling of interhemispheric connections. The z-scored connectivity between MTL regions is used as the edge weight. To assess the significance of a hub, we used edge weights derived from each of the 250 null networks, generated by shuffling the original trial labels (see “Network analyses”). For each region, the true node strength is compared to the distribution of null node strengths to derive a z-score or p-value. In Figure 2, p-values were Benjamini-Hochberg corrected for multiple comparisons and thresholded at $P < 0.05$.

Phase lag analysis—To assess the magnitude of phase lags between MTL subregions (Figure S2, Figure S3), we measured the mean absolute phase lag across all electrode pairs and encoding/retrieval trials in successful and unsuccessful memory conditions, separately. The result was a distribution of mean phase lags (between 0 and 90 degrees) across all electrode pairs that span a given MTL region-pair (Figure S2-A and Figure S2-C), for each memory condition. Any pair that did not pass a Rayleigh test for nonuniformity was excluded ($P < 0.05$; the majority of electrode pairs for both memory conditions and region-pairs met this condition). We further binned each electrode pair according to the magnitude of its mean phase lag in the unsuccessful memory condition; “zero” (0-5 degrees), and small/medium/large, which are the terciles of all 5+ degree lags. For each bin, we used a

paired t-test to ask whether phase lags significantly changed between successful (blue) and unsuccessful (red) conditions. Next, we used a 2-sample *t*-test to ask whether, in the remembered condition, phase synchronization (e.g. PLV z-score, see "Data analyses and spectral methods") systematically differed between electrode pairs with zero (0-5 degree lags) and nonzero mean phase lags (Figure S2-B and Figure S2-D). Finally, to confirm these results, we used the circular *m*-test, equivalent to a 1-sample *t*-test, to ask whether the distribution of phase lags for each electrode pair significantly differed from zero ($P < 0.05$ threshold, pycircstat library [65]; Figure S3). We used a binomial test to ask whether the count of such pairs significantly differed from chance. We further used a 2-sample *t*-test to assess whether PLV *z*-scores significantly differ between electrode pairs with zero vs. nonzero lag distributions.

Analysis of spectral power—To determine the change in spectral power associated with successful memory encoding or retrieval, we convolve each electrode's signal with complex-valued Morlet wavelets (6 cycles) to obtain power information. For high-frequency activity (HFA) we used 13 wavelets spaced 5 Hz (30-90 Hz). Frequencies, time windows, buffers, and spectral methods are otherwise identical to those used in the earlier phase-based analysis (see "Data analyses and spectral methods").

For each electrode in each subject, we log transformed and z-scored power within each session of the free-recall task, which comprises approximately 300 trials. Power values were next averaged into non-overlapping 100 ms time bins spanning the trial. To assess the statistical relationship between power and later recollection of a word (the power SME), power values for each electrode, trial, time, and frequency were separated into two distributions according to whether the word was later or not remembered, a Welch's t-test was performed to compare the means of the two distributions. The resulting t-statistics were averaged across electrodes that fell in a common MTL region (either hippocampal subfields or MTL cortices), generating an average t-statistic per subject. Finally, for all MTL regions with more than 5 subjects' worth of data, we performed a 1-sample t-test on the distribution of t-statistics against zero. The result is a t-statistic that reflects the successful encoding-related change in power across subjects. We report these t-statistics in time-frequency plots in Figure 7B, along with time-averaged t-statistics in Figure 7A (encoding, 400-1100 ms; retrieval, −500-0 ms).

Retrieval analysis—To find out whether functional connectivity networks uncovered in the memory encoding contrast generalized to different cognitive operations, we further analyzed connectivity in a retrieval contrast. This was done in a manner similar to Burke, et al. 2014 as follows:

For each subject, we identified any 1000 ms period preceding vocal onset of a successfully recalled word, so long as that word was not preceded or followed by any other vocalization for at least 2 seconds. For each retrieval event, we then searched for a 1000 ms interval from a different list during which no successful retrieval (or vocalization) took place, occurring at the same time as the original recall relative to the beginning of the recall period (30-second recall periods followed each of 25 lists per session). These 1000 ms intervals are called "deliberation" intervals, reflecting a time during which a subject was liable to be attempting

recall. If no match could be found for the exact time of a given recall, we searched for, still from a different list, a matched deliberation interval within 2 seconds surrounding the onset time of the retrieval event. If no match was available within 2 seconds, the original recall event was discarded from analysis. In this way, each successful retrieval is matched with exactly one deliberation interval, of equal length, from a different recall list.

Analyses of the retrieval contrast were otherwise treated identically to analyses of the encoding contrast, described in “Data analyses and spectral methods.”

Supplementary Material

Refer to Web version on PubMed Central for supplementary material.

Acknowledgements

We thank Blackrock Microsystems for providing neural recording equipment. This work was supported by the DARPA Restoring Active Memory (RAM) program (Cooperative Agreement N66001-14-2-4032), as well as National Institutes of Health grant MH55687 and T32NS091006. We are indebted to all patients who have selflessly volunteered their time to participate in our study. The views, opinions, and/or findings contained in this material are those of the authors and should not be interpreted as representing the official views or policies of the Department of Defense or the U.S. Government. We also thank Dr. James Kragel for providing valuable feedback on this work.

References

1. Eichenbaum H (2000). A cortical-hippocampal system for declarative memory. Nat. Rev. Neurosci 1, 41–50. [PubMed: 11252767]
2. Paller KA, and Wagner AD (2002). Observing the transformation of experience into memory. Trends Cogn. Sci 6, 93–102. [PubMed: 15866193]
3. Solomon EA, Kragel JE, Sperling MR, Sharan A, Worrell G, Kucewicz M, Inman CS, Lega B, Davis KA, Stein JM, et al. (2017). Widespread theta synchrony and high-frequency desynchronization underlies enhanced cognition. Nat. Commun 8, 1704. [PubMed: 29167419]
4. Ranganath C, Heller A, Cohen MX, Brozinsky CJ, and Rissman J (2005). Functional connectivity with the hippocampus during successful memory formation. Hippocampus 15, 997–1005. [PubMed: 16281291]
5. Vincent JL, Snyder AZ, Fox MD, Shannon BJ, Andrews JR, Raichle ME, and Buckner RL (2006). Coherent Spontaneous Activity Identifies a Hippocampal-Parietal Memory Network. J. Neurophysiol 96, 3517–3531. [PubMed: 16899645]
6. Fell J, and Axmacher N (2011). The role of phase synchronization in memory processes. Nat. Rev. Neurosci 12, 105–118. [PubMed: 21248789]
7. Eichenbaum H, Otto T, and Cohen NJ (1992). The hippocampus--what does it do? Behav. Neural Biol 57, 2–36. [PubMed: 1567331]
8. Eichenbaum H, Yonelinas AP, and Ranganath C (2007). The medial temporal lobe and recognition memory. Annu. Rev. Neurosci 30, 123–52. [PubMed: 17417939]
9. Wagner AD, Schacter DL, Rotte M, Koutstaal W, Maril A, Dale AM, Rosen BR, and Buckner RL (1998). Building memories: remembering and forgetting of verbal experiences as predicted by brain activity. Science 281, 1188–91. [PubMed: 9712582]
10. Buzsáki G (2002). Theta Oscillations in the Hippocampus. Neuron 33, 325–340. [PubMed: 11832222]
11. Moser EI, Kropff E, and Moser M-B (2008). Place Cells, Grid Cells, and the Brain’s Spatial Representation System. Annu. Rev. Neurosci 31, 69–89. [PubMed: 18284371]
12. MacDonald CJ, Lepage KQ, Eden UT, and Eichenbaum H (2011). Hippocampal “time cells” bridge the gap in memory for discontiguous events. Neuron 71, 737–749. [PubMed: 21867888]

13. Yamamoto J, Suh J, Takeuchi D, and Tonegawa S (2014). Successful Execution of Working Memory Linked to Synchronized High-Frequency Gamma Oscillations. Cell 157, 845–857. [PubMed: 24768692]
14. Montgomery SM, and Buzsáki G (2007). Gamma oscillations dynamically couple hippocampal CA3 and CA1 regions during memory task performance. Proc. Natl. Acad. Sci. U. S. A 104, 14495–500. [PubMed: 17726109]
15. Schomburg EW, Fernández-Ruiz A, Mizuseki K, Berényi A, Anastassiou CA, Koch C, and Buzsáki G (2014). Theta Phase Segregation of Input-Specific Gamma Patterns in Entorhinal-Hippocampal Networks. Neuron 84, 470–485. [PubMed: 25263753]
16. Seidenbecher T, Laxmi TR, Stork O, and Pape H-C (2003). Amygdalar and hippocampal theta rhythm synchronization during fear memory retrieval. Science 307, 846–50.
17. Colgin LL (2016). Rhythms of the hippocampal network. Nat. Rev. Neurosci 77. [PubMed: 26806627]
18. Hasselmo ME, and Eichenbaum H (2005). Hippocampal mechanisms for the context-dependent retrieval of episodes. Neural Netw 18, 1172–90. [PubMed: 16263240]
19. Diana RA, Yonelinas AP, and Ranganath C (2007). Imaging recollection and familiarity in the medial temporal lobe: a three-component model. Trends Cogn. Sci 11, 379–386. [PubMed: 17707683]
20. Burgess N, Maguire EA, and O'Keefe J (2002). The Human Hippocampus and Spatial and Episodic Memory. Neuron 35, 625–641. [PubMed: 12194864]
21. Fell J, Klaver P, Lehnertz K, Grunwald T, Schaller C, Elger CE, and Fernández G (2001). Human memory formation is accompanied by rhinal-hippocampal coupling and decoupling. Nat. Neurosci 4, 1259–64. [PubMed: 11694886]
22. Fell J, Ludowig E, Rosburg T, Axmacher N, and Elger CE (2008). Phase-locking within human mediotemporal lobe predicts memory formation. Neuroimage 43, 410–419. [PubMed: 18703147]
23. Fell J, Klaver P, Elfadil H, Schaller C, Elger CE, and Fernández G (2003). Rhinal-hippocampal theta coherence during declarative memory formation: interaction with gamma synchronization? Eur. J. Neurosci 17, 1082–1088. [PubMed: 12653984]
24. Lega BC, Jacobs J, and Kahana M (2012). Human hippocampal theta oscillations and the formation of episodic memories. Hippocampus 22, 748–761. [PubMed: 21538660]
25. Kahana MJ, Seelig D, and Madsen JR (2001). Theta returns. Curr. Opin. Neurobiol 11, 739–744. [PubMed: 11741027]
26. Lin J-J, Rugg MD, Das S, Stein J, Rizzuto DS, Kahana MJ, and Lega BC (2017). Theta band power increases in the posterior hippocampus predict successful episodic memory encoding in humans. Hippocampus 27, 1040–1053. [PubMed: 28608960]
27. Greenberg JA, Burke JF, Haque R, Kahana MJ, and Zaghloul KA (2015). Decreases in theta and increases in high frequency activity underlie associative memory encoding. Neuroimage 114, 257–63. [PubMed: 25862266]
28. Burke JF, Sharan AD, Sperling MR, Ramayya AG, Evans JJ, Healey MK, Beck EN, Davis KA, Lucas TH, and Kahana MJ (2014). Theta and high-frequency activity mark spontaneous recall of episodic memories. J. Neurosci 34, 11355–65. [PubMed: 25143616]
29. Buzsáki G, and Moser EI (2013). Memory, navigation and theta rhythm in the hippocampal-entorhinal system. Nat. Neurosci 16, 130–138. [PubMed: 23354386]
30. Buzsáki G, and Schomburg EW (2015). What does gamma coherence tell us about inter-regional neural communication? Nat. Neurosci 18, 484–489. [PubMed: 25706474]
31. Rutishauser U, Ross IB, Mamelak AN, and Schuman EM (2010). Human memory strength is predicted by theta-frequency phase-locking of single neurons. Nature 464, 903–907. [PubMed: 20336071]
32. Watrous AJ, Tandon N, Conner CR, Pieters T, and Ekstrom AD (2013). Frequency-specific network connectivity increases underlie accurate spatiotemporal memory retrieval. Nat. Neurosci 16, 349–56. [PubMed: 23354333]
33. Colgin LL (2013). Mechanisms and Functions of Theta Rhythms. Annu. Rev. Neurosci 36, 295–312. [PubMed: 23724998]

34. Sarnthein J, Petsche H, Rappelsberger P, Shaw GL, and von Stein A (1998). Synchronization between prefrontal and posterior association cortex during human working memory. Proc. Natl. Acad. Sci. U. S. A 95, 7092–6. [PubMed: 9618544]
35. Clouter A, Shapiro KL, and Hanslmayr S (2017). Theta Phase Synchronization Is the Glue that Binds Human Associative Memory. Curr. Biol 27, 3143–3148.e6. [PubMed: 28988860]
36. Backus AR, Schoffelen JM, Szebenyi S, Hanslmayr S, and Doeller CF (2016). Hippocampal-prefrontal theta oscillations support memory integration. Curr. Biol 26.
37. Burke JF, Long NM, Zaghloul KA, Sharan AD, Sperling MR, and Kahana MJ (2014). Human intracranial high-frequency activity maps episodic memory formation in space and time. Neuroimage 85, 834–843. [PubMed: 23827329]
38. Kragel JE, Ezzyat Y, Sperling MR, Gorniak R, Worrell GA, Berry BM, Inman C, Lin J-J, Davis KA, Das SR, et al. (2017). Similar patterns of neural activity predict memory function during encoding and retrieval. Neuroimage 155, 60–71. [PubMed: 28377210]
39. Long NM, Sperling MR, Worrell GA, Davis KA, Gross RE, Lega BC, Jobst BC, Sheth SA, Zaghloul K, Stein JM, et al. (2017). Contextually Mediated Spontaneous Retrieval Is Specific to the Hippocampus. Curr. Biol 27, 1074–1079. [PubMed: 28343962]
40. Lachaux JP, Rodriguez E, Martinerie J, and Varela FJ (1999). Measuring phase synchrony in brain signals. Hum. Brain Mapp 8, 194–208. [PubMed: 10619414]
41. Squire LR, Stark CEL, and Clark RE (2004). THE MEDIAL TEMPORAL LOBE. Annu. Rev. Neurosci 27, 279–306. [PubMed: 15217334]
42. Davachi L (2006). Item, context and relational episodic encoding in humans. Curr. Opin. Neurobiol 16, 693–700. [PubMed: 17097284]
43. Kloosterman F, Witter MP, and Van Haeften T (2003). Topographical and laminar organization of subicular projections to the parahippocampal region of the rat. J. Comp. Neurol 455, 156–171. [PubMed: 12454982]
44. Liang JC, and Preston AR (2015). Medial Temporal Lobe Subregional Function in Human Episodic Memory In The Wiley Handbook on the Cognitive Neuroscience of Memory (Chichester, UK: John Wiley & Sons, Ltd), pp. 108–130.
45. Vinck M, Oostenveld R, van Wingerden M, Battaglia F, and Pennartz CMA (2011). An improved index of phase-synchronization for electrophysiological data in the presence of volume-conduction, noise and sample-size bias. Neuroimage 55, 1548–1565. [PubMed: 21276857]
46. Bastos AM, and Schoffelen J-M (2015). A Tutorial Review of Functional Connectivity Analysis Methods and Their Interpretational Pitfalls. Front. Syst. Neurosci 9, 175. [PubMed: 26778976]
47. Yassa MA, and Stark CEL (2011). Pattern separation in the hippocampus. Trends Neurosci 34, 515–525. [PubMed: 21788086]
48. Diana RA, Yonelinas AP, and Ranganath C (2010). Medial temporal lobe activity during source retrieval reflects information type, not memory strength. J. Cogn. Neurosci 22, 1808–18. [PubMed: 19702458]
49. Merkow MB, Burke JF, and Kahana MJ (2015). The human hippocampus contributes to both the recollection and familiarity components of recognition memory. Proc. Natl. Acad. Sci. U. S. A 112, 14378–83. [PubMed: 26578784]
50. Burke JF, Ramayya AG, Kahana MJ, Rgy G, Ki B, and Freeman W (2015). Human intracranial high-frequency activity during memory processing: neural oscillations or stochastic volatility? This review comes from a themed issue on Brain rhythms and dynamic coordination. Curr. Opin. Neurobiol 31, 104–110. [PubMed: 25279772]
51. Burke JF, Zaghloul KA, Jacobs J, Williams RB, Sperling MR, Sharan AD, and Kahana MJ (2013). Synchronous and asynchronous theta and gamma activity during episodic memory formation. J. Neurosci 33, 292–304. [PubMed: 23283342]
52. Igarashi KM, Lu L, Colgin LL, Moser M-B, and Moser EI (2014). Coordination of entorhinal-hippocampal ensemble activity during associative learning. Nature 510, 143–147. [PubMed: 24739966]
53. Fell J, Klaver P, Lehnertz K, Grunwald T, Schaller C, Elger CE, and Fernández G (2001). Human memory formation is accompanied by rhinal-hippocampal coupling and decoupling.

54. Bieri KW, Bobbitt KN, and Colgin LL (2014). Slow and Fast Gamma Rhythms Coordinate Different Spatial Coding Modes in Hippocampal Place Cells. Neuron 82, 670–681. [PubMed: 24746420]
55. Colgin LL, Denninger T, Fyhn M, Hafting T, Bonnevie T, Jensen O, Moser MB, and Moser EI (2009). Frequency of gamma oscillations routes flow of information in the hippocampus. Nature 462, 353–357. [PubMed: 19924214]
56. Miller J, Watrous AJ, Tsitsiklis M, Lee SA, Sheth SA, Schevon CA, Smith EH, Sperling MR, Sharan A, Asadi-Pooya AA, et al. (2018). Lateralized hippocampal oscillations underlie distinct aspects of human spatial memory and navigation. Nat. Commun 9, 2423. [PubMed: 29930307]
57. Lisman JE, and Jensen O (2013). The Theta-Gamma Neural Code. Neuron 77, 1002–1016. [PubMed: 23522038]
58. Hasselmo ME, Bodelón C, and Wyble BP (2002). A Proposed Function for Hippocampal Theta Rhythm: Separate Phases of Encoding and Retrieval Enhance Reversal of Prior Learning. Neural Comput 14, 793–817. [PubMed: 11936962]
59. Cohen MX (2015). Effects of time lag and frequency matching on phase-based connectivity. J. Neurosci. Methods 250, 137–146. [PubMed: 25234308]
60. Yushkevich PA, Pluta JB, Wang H, Xie L, Ding S-L, Gertje EC, Mancuso L, Kliot D, Das SR, and Wolk DA (2015). Automated volumetry and regional thickness analysis of hippocampal subfields and medial temporal cortical structures in mild cognitive impairment. Hum. Brain Mapp 36, 258–87. [PubMed: 25181316]
61. Avants BB, Epstein CL, Grossman M, and Gee JC (2008). Symmetric diffeomorphic image registration with cross-correlation: Evaluating automated labeling of elderly and neurodegenerative brain. Med. Image Anal 12, 26–41. [PubMed: 17659998]
62. Moore M, Hu Y, Woo S, O'Hearn D, Iordan AD, Dolcos S, and Dolcos F (2014). A comprehensive protocol for manual segmentation of the medial temporal lobe structures. J. Vis. Exp
63. Gramfort A, Luessi M, Larson E, Engemann DA, Strohmeier D, Brodbeck C, Parkkonen L, and Hamalainen MS (2014). MNE software for processing MEG and EEG data. Neuroimage 86, 446–460. [PubMed: 24161808]
64. Rubinov M, and Sporns O (2010). Complex network measures of brain connectivity: Uses and interpretations. Neuroimage 52, 1059–1069. [PubMed: 19819337]
65. Berens P (2009). CircStat: A *MATLAB* Toolbox for Circular Statistics. J. Stat. Softw 31, 1–21.

Highlights

- We assessed intra-MTL connectivity during a memory task in 131 epilepsy patients.
- Successful encoding and retrieval were correlated with elevated theta connectivity.
- Left entorhinal cortex emerged as a hub of intra-MTL connectivity.
- We found broad increases in high-frequency power but decreases in theta power.

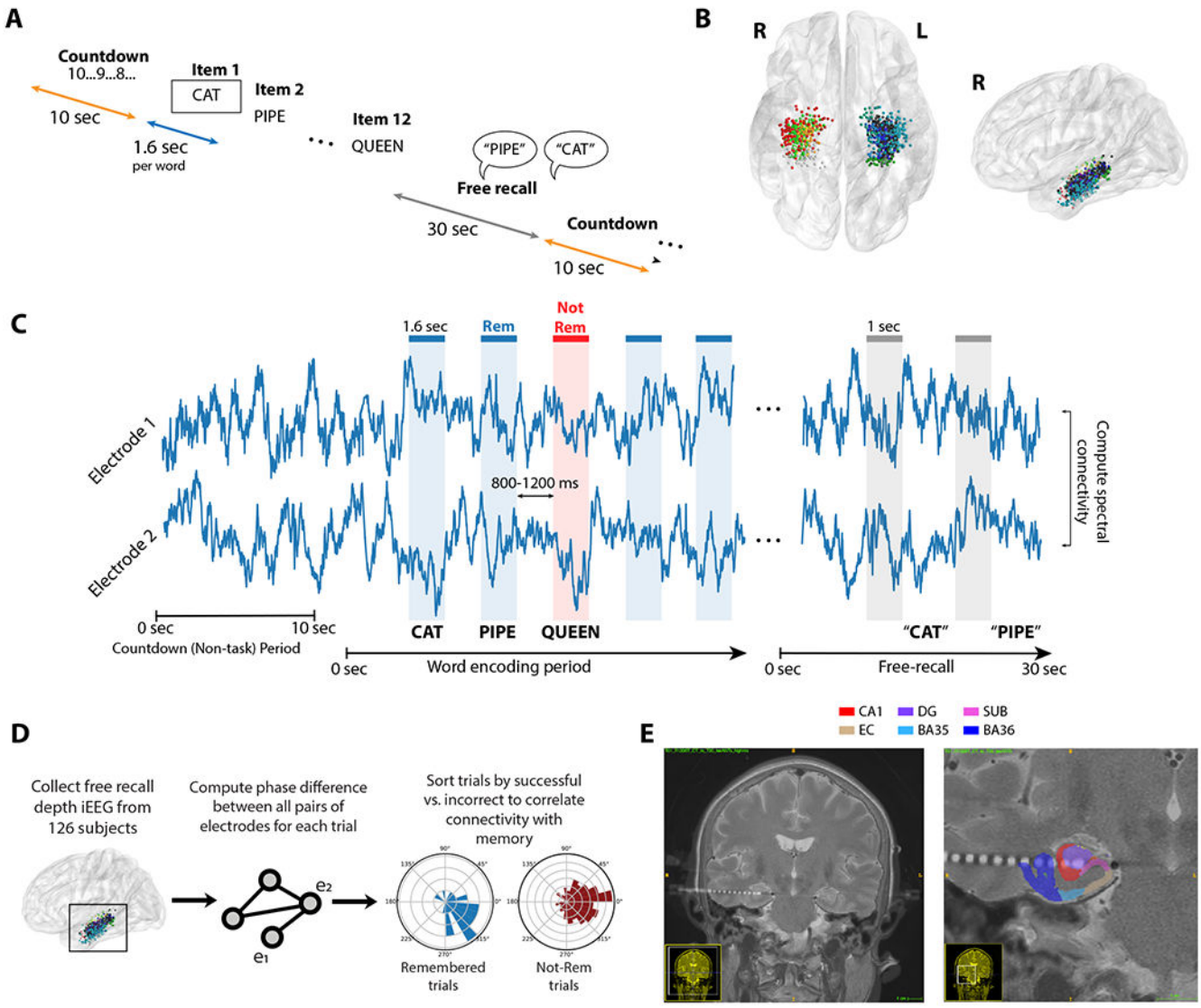

Figure 1. Task structure and analysis methods.

A. Subjects performed a verbal free-recall task, consisting of alternating periods of pre-list countdowns (orange), word encoding (blue), and free-recall (gray). See Methods for details. **B.** 131 subjects with indwelling electrodes in the medial temporal lobe (MTL) participated. Electrodes were localized to CA1, dentate gyrus (DG), subiculum (Sub), perirhinal cortex (PRC), entorhinal cortex (EC), or parahippocampal cortex (PHC). Each dot shows an electrode in this dataset, colored by MTL subregion. **C.** To construct networks of intra-MTL activity, we used the PLV to analyze phase differences between electrode pairs. Time windows in two conditions were analyzed: 1.6-second epochs during word encoding (blue/red), and 1-second periods leading up to recall vocalizations (gray). **D.** To assess intra-MTL connectivity, phase differences were computed for each electrode pair in all trials, and trials were then sorted by successful vs. unsuccessful memory. PLV was computed for each distribution, and a nonparametric permutation procedure was used to determine whether connectivity is significantly different between distributions. Connectivity values were

averaged across electrode pairs and subjects to yield the final MTL network maps depicted in Figure 2 (see Methods for details). **E.** Example subject MRI with post-operative CT and segmentations overlaid to demonstrate placement of depth electrodes in the MTL. See Figure S1-B for additional examples. BA35/36 were combined to form our PRC label. See also Figure S1 and Table S1.

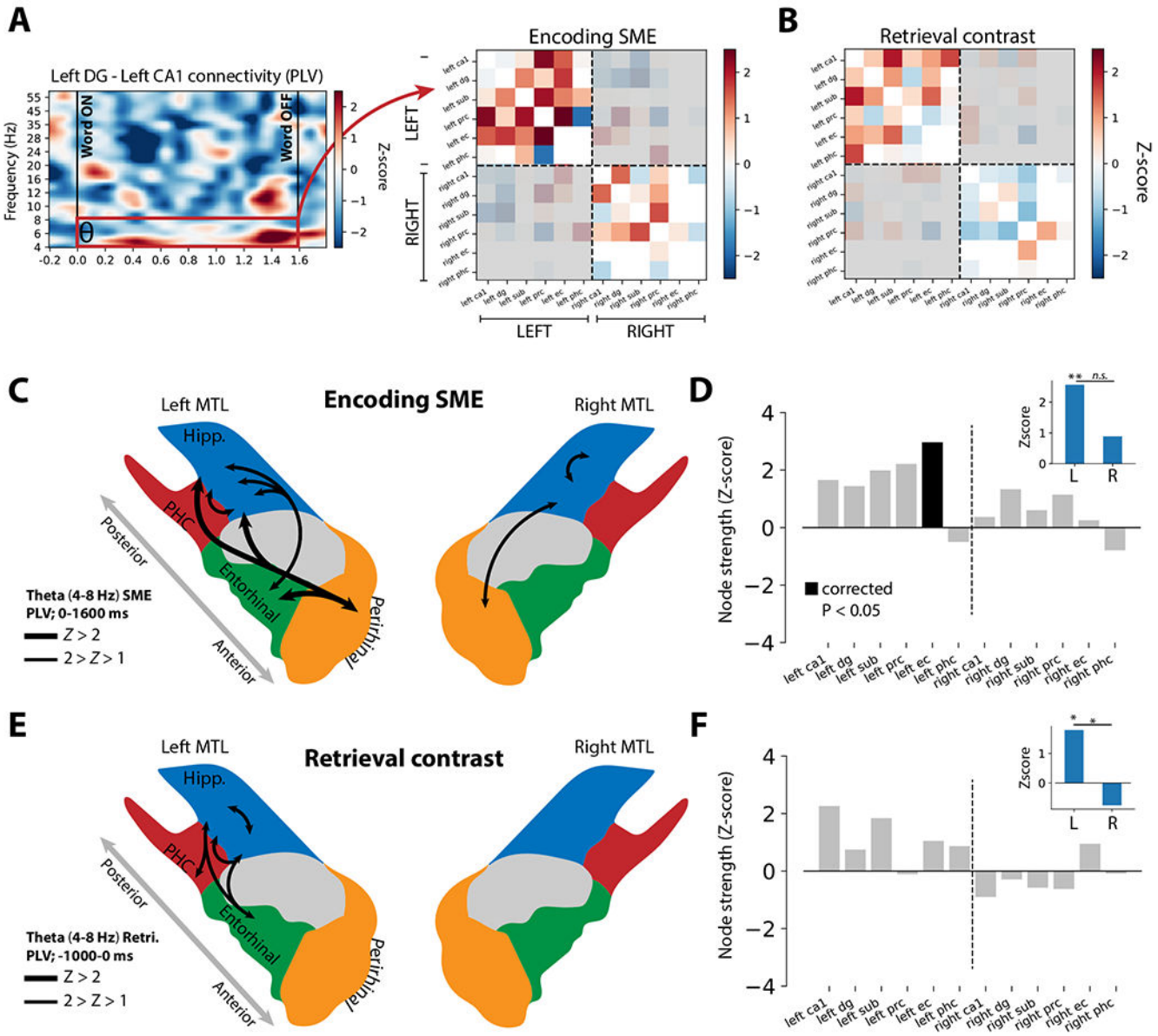

Figure 2. Structure of theta networks supporting episodic memory.

A. To determine overall connectivity for each pair of MTL subregions, PLV was averaged over the encoding (word presentation, 0-1.6 seconds) or retrieval (−1.0 to 0 seconds prior to retrieval onset) intervals, yielding a single z-scored connection weight. (see Methods for details). The matrix representation of all these weights is called an adjacency matrix, shown here for the encoding contrast in the theta band (4-8 Hz). Any inter-regional connection with fewer than 5 subjects' worth of data is excluded from analysis (white cells). Because interhemispheric connections are less well sampled than intra-hemispheric connections (Figure S1), and because interhemispheric connectivity is largely asynchronous, they are excluded from this analysis of network structure (gray shading). **B.** Retrieval contrast theta adjacency matrix, organized as in (A). **C.** Depiction of strongest ($Z > 1$) synchronous PLV connectivity in the SME contrast, derived from the theta adjacency matrix in (A). These

connections reflect the averaged connection strength over the word presentation interval (0.0-1.6 seconds; see Methods for details). Thicker lines reflect Z-scores above 2. **D.** Z-scored node strength for each MTL region, computed only for connections to ipsilateral MTL regions (see Methods for details). Node strength indicates the sum of all connections to a given region, with positive Z-scores indicating enhanced overall connectivity to a given region during successful encoding epochs (a “hub” of connectivity). Left EC exhibited significant positive node strength (FDR-corrected permuted $P < 0.05$) correlated with words that were successfully remembered. **Inset:** Z-scored total network strength for all intra-hemispheric MTL connections, computed by summing the connection weights for each hemisphere’s MTL subregions separately. Intra-MTL connections on the left are significantly greater than chance ($P = 0.005$), and trend greater than right-sided connections ($P = 0.15$). **E.** Schematic of strongest theta retrieval connections, reflecting increased PLV between two MTL subregions in the 1-second immediately prior to successful retrieval of a word item. **F.** Same as (D), but reflecting synchronous activity from the 1-second period prior to successful retrieval of a word item. No region exhibits a significant node strength after correction for multiple comparisons, but left CA1 is significant if uncorrected ($P = 0.013$). **Inset:** Z-scored total network strength for all intra-hemispheric MTL connections. Left-sided connections are significantly greater than chance ($P = 0.04$) and significantly greater than right-sided connections ($P = 0.03$).

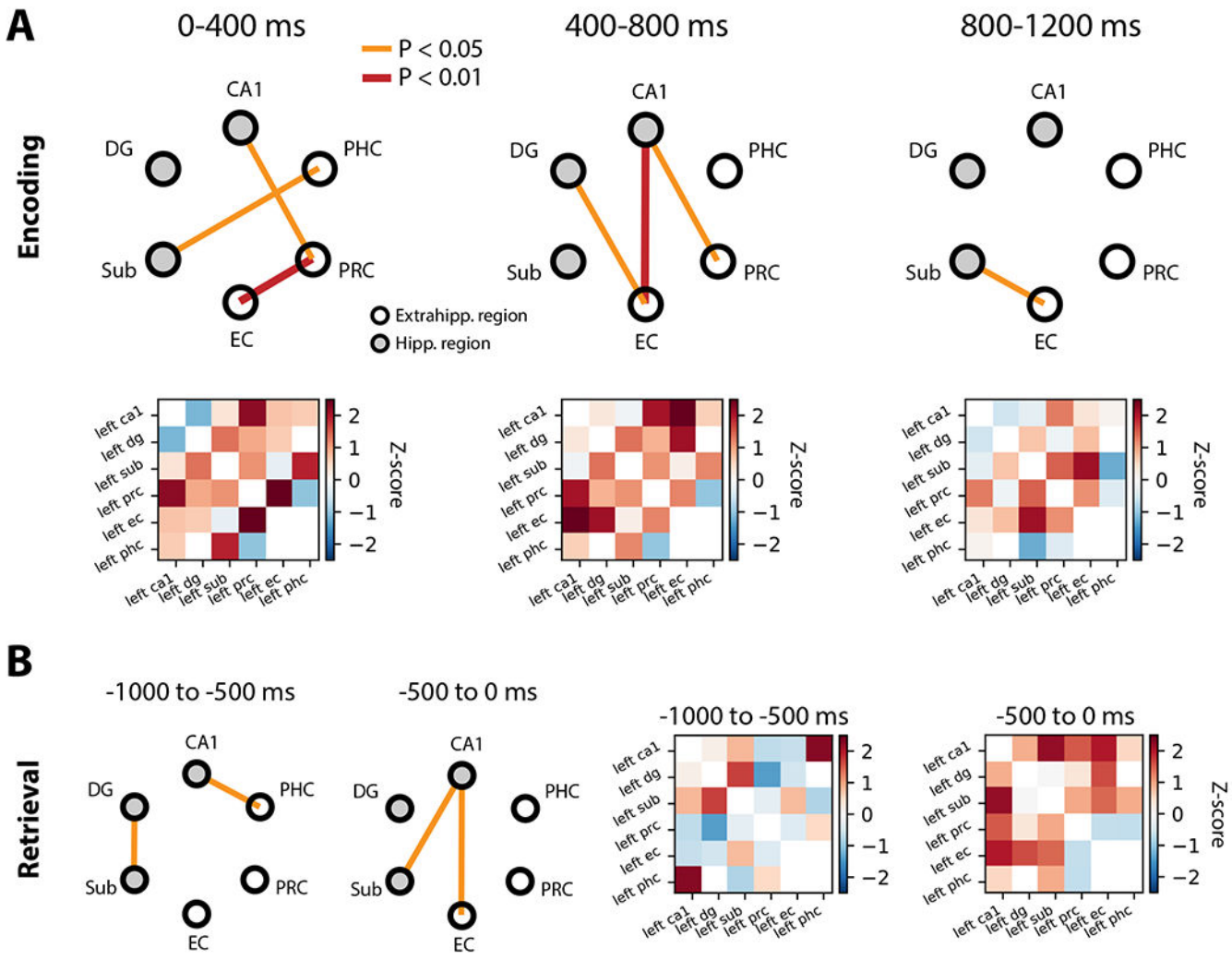

Figure 3. Time-varying dynamics of memory-related synchronization in the left MTL.

A. Theta synchronization during early (0-400 ms), middle (400-800 ms) and late (800-1200 ms) epochs of the encoding interval, during which words to be remembered are presented on the screen. *Top*: Schematic representation of synchronization among left MTL subregions, contrasting successful vs. unsuccessful encoding (i.e. encoding SME). Yellow lines indicate connections of permuted $P < 0.05$ significance; red lines indicate $P < 0.01$ significance. *Bottom*: Adjacency matrix representation of the encoding SME in the left MTL; red colors indicate a relative synchronization for successful encoding events. **B.** Theta synchronization during early (1000 to −500 ms) and late (−500 to 0 ms) epochs of the pre-retrieval period, relative to matched deliberation intervals. Structured as in (A).

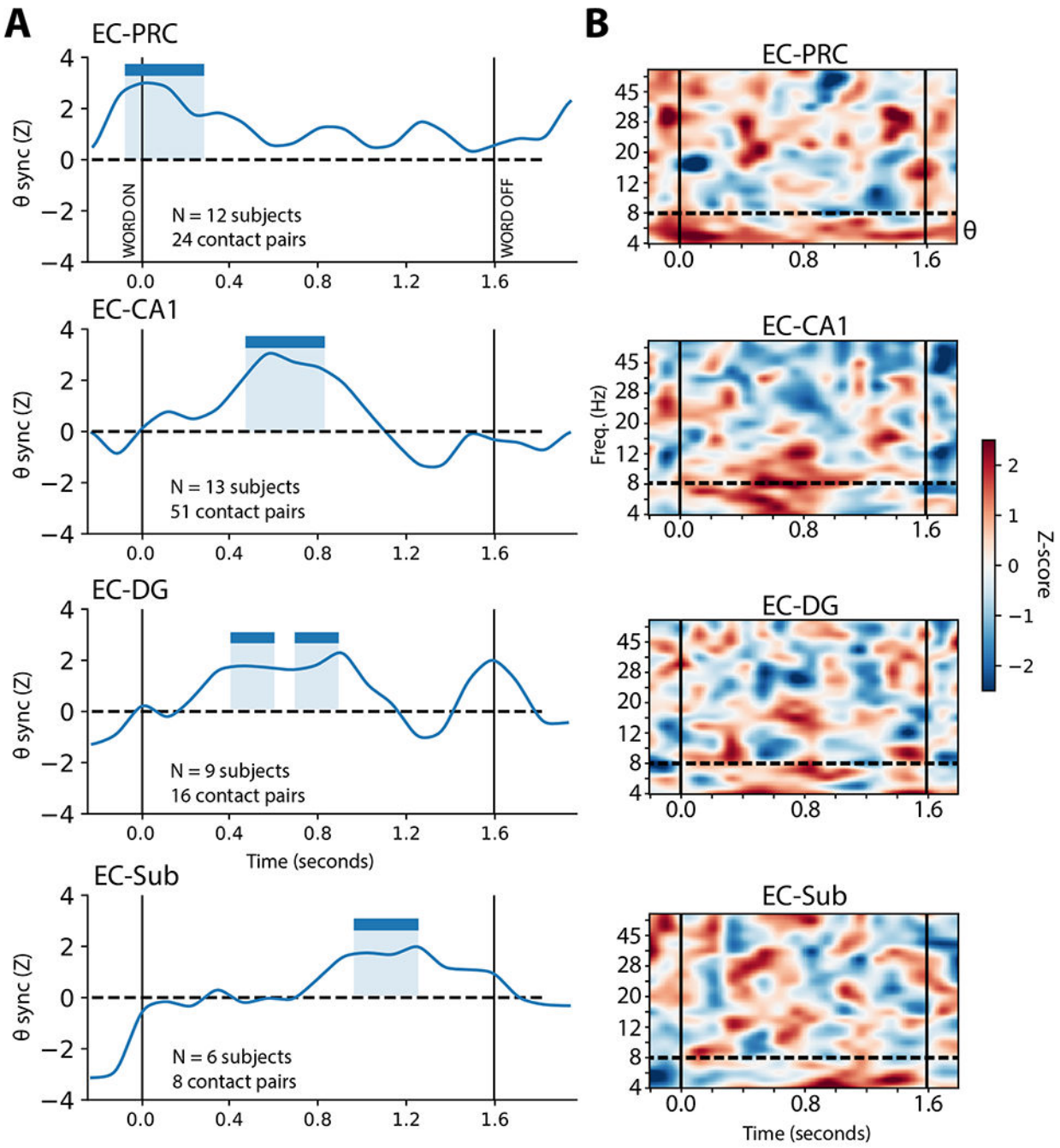

Figure 4. Timing analysis of key encoding connections to the left EC.

A. The timecourse of encoding-related synchronization is depicted for each connection where significant connectivity was observed in the average (see Figure 3). Blue shaded areas are indicated wherever two or more consecutive $P < 0.05$ time windows occur (see Methods for details). **B.** Time-frequency spectrogram contrasts, averaged over subjects, for each significant EC connection. Vertical lines indicate word onset. See also Figure S2, Figure S3, and Figure S4.

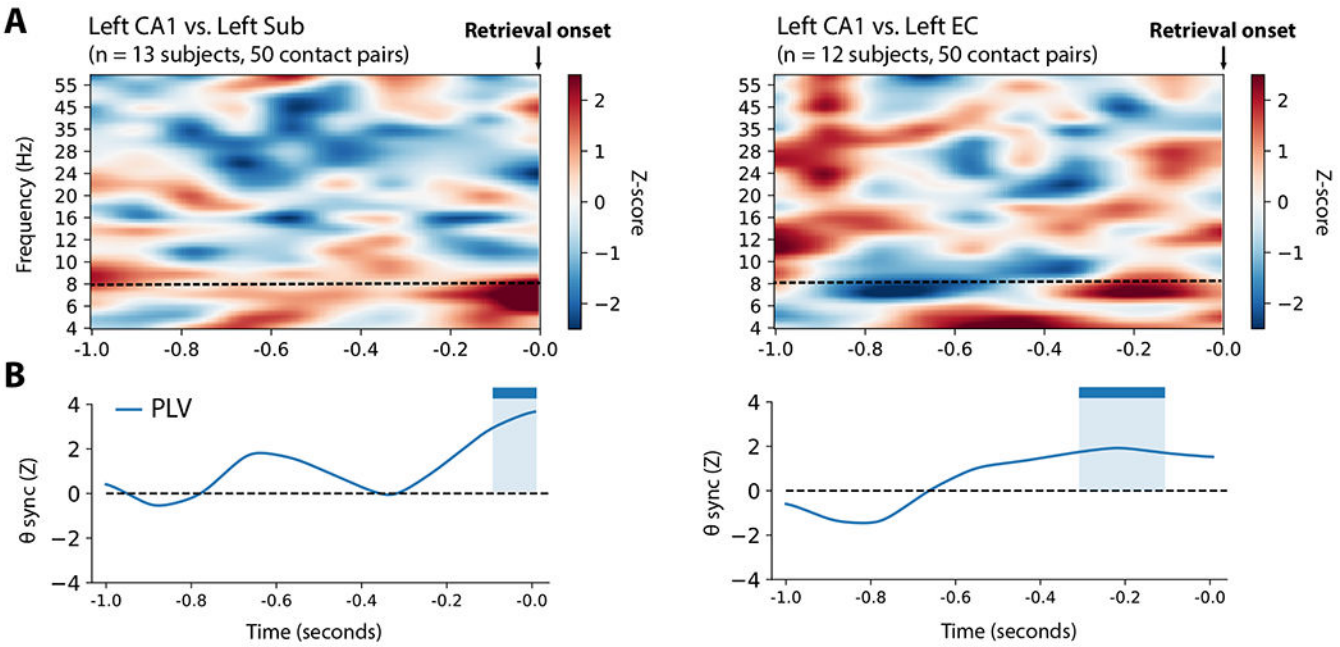

Figure 5. Timing analysis of key retrieval connections.

A. *Left:* Time-frequency spectrogram of left CA1-subiculum PLV synchronization in the retrieval contrast, averaged across subjects. *Right:* Time-frequency spectrogram of left CA1-EC PLV synchronization in the retrieval contrast. **B.** *Left:* Timecourse of left CA1-subiculum PLV synchronization, organized as in Figure 4B. Significant ($P < 0.05$) PLV synchronization is marked from −200 to 0 ms prior to recall onset. *Right:* Timecourse of left CA1-EC synchronization. Significant PLV synchronization is marked from −300 to −100 ms prior to recall onset. See also Figure S2.

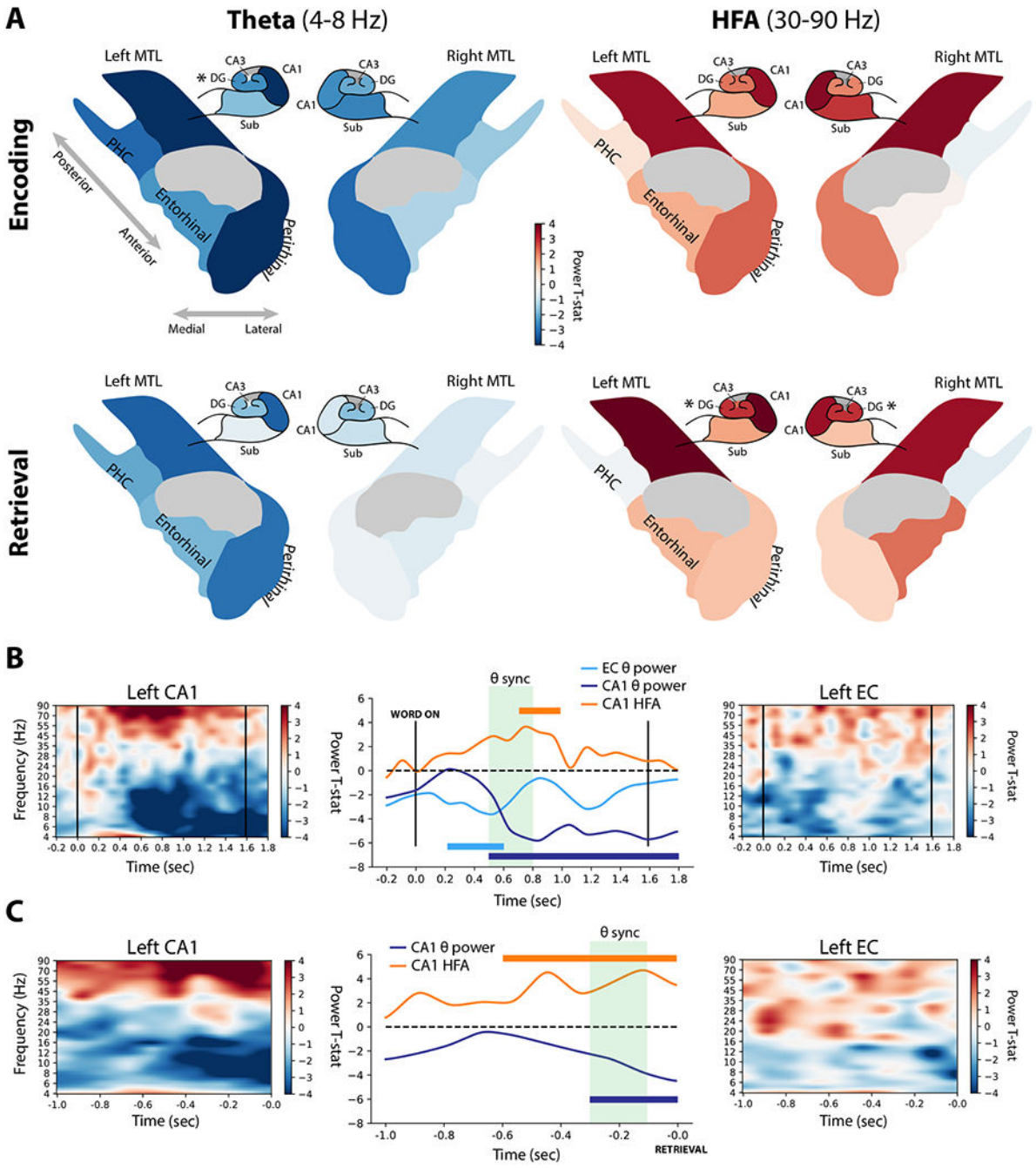

Figure 6. Dynamics of spectral power associated with memory encoding and retrieval.

A. For each MTL subregion and hippocampal subfield, the spectral power during successful vs. unsuccessful encoding or retrieval epochs was computed in the theta (4-8 Hz) and high-frequency activity (30-90 Hz) bands. For encoding periods, powers were averaged in the 400-1100 ms interval, and between −500-0 ms for retrieval periods, which were the times featuring the most prominent network-wide power change (see Methods for details). The t-statistic indicating the relative power during successful versus unsuccessful encoding or retrieval is mapped to a color, with reds indicating increased power and blues indicating

decreased power. These colors are displayed on schematics of MTL and hippocampal anatomy for encoding and retrieval conditions (rows), and theta or HFA bands (columns). Asterisks indicate significant ($P < 0.05$) memory-related power modulation, FDR corrected across tested regions. “Hipp” was not tested collectively but is colored according to CA1. **B.** Left CA1 ($N = 19$) and left EC ($N = 57$) showed changes in spectral power that were temporally associated with enhanced connectivity between the regions (see Figure 5B). Significant ($P < 0.05$) increases in CA1 HFA occurred from 700-1000 ms after word onset, while CA1 theta power decreased from 500 ms to the end of the word encoding interval. Left EC theta power decreased from 200-600 ms. The period of significantly enhanced theta PLV is marked in green. **C.** Organized as (B), but for the EC-CA1 interactions in the retrieval contrast. No significant modulations of left EC power were observed in the pre-recall interval. See also Figure S5.

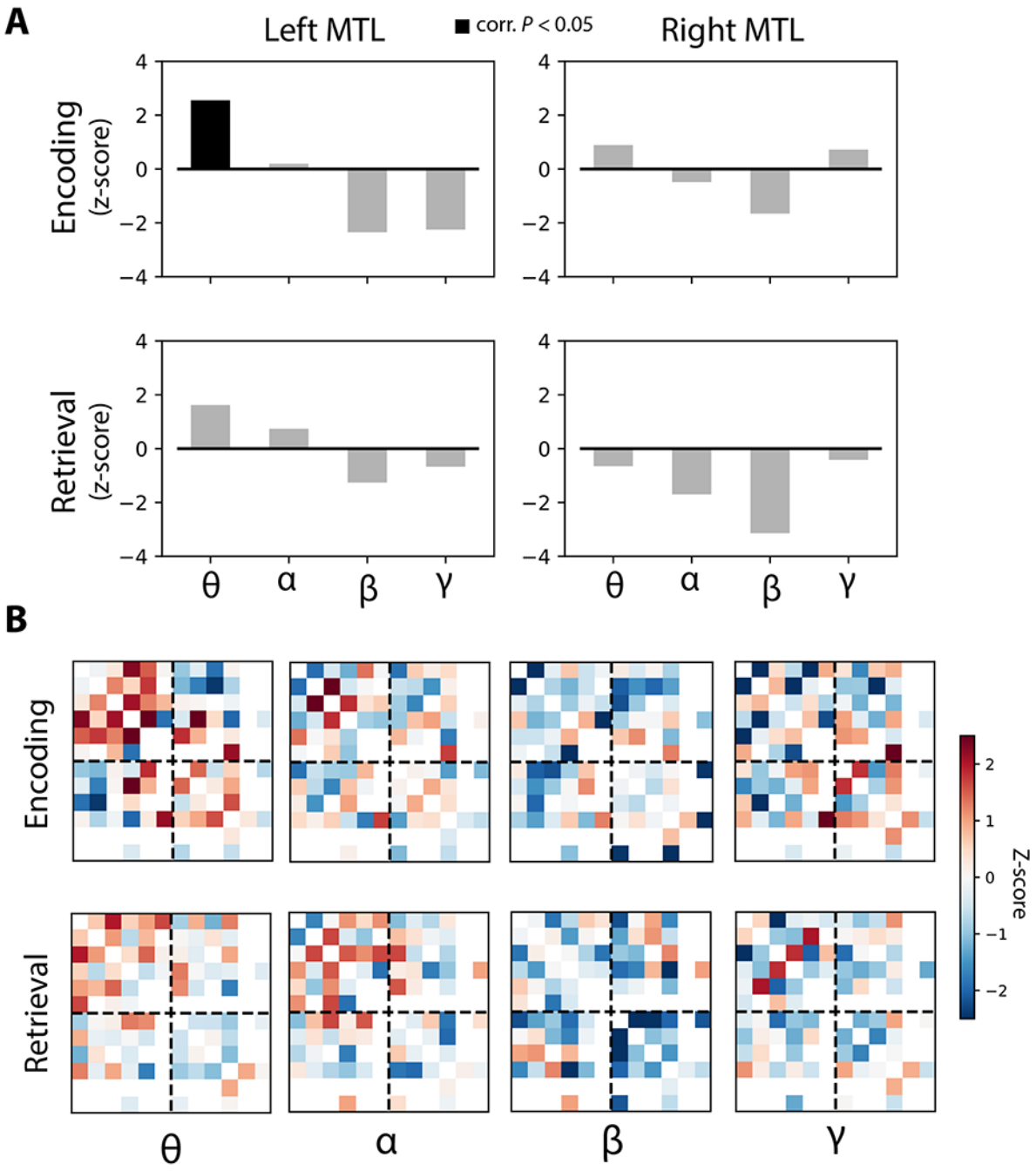

Figure 7. Network-wide synchrony by frequency band.

A. Network-wide synchronization is computed by averaging all inter-regional connection weights within the right and left MTL, for each task contrast, and comparing the average to a null distribution (see Methods for details). Network-wide synchronization was observed in the left MTL in the theta band for the encoding contrast, FDR-corrected for multiple comparisons (permuted $P < 0.05$). **B.** Adjacency matrix representation of the MTL network

for each frequency band and task contrast. Red colors indicate a memory-related synchronization. Matrices organized as in Figure 2. See also Figure S4 and Figure S6.